Effect of Bed Size on Hydrodynamics in 3-D Gas–Solid Fluidized Beds

Vikrant Verma, Johan T. Padding, Niels G. Deen, and J. A. M. (Hans) Kuipers
Dept. of Chemical Engineering and Chemistry, Eindhoven University of Technology, PO Box 513, 5600 MB Eindhoven, The Netherlands

DOI 10.1002/aic.14738
Published online February 6, 2015 in Wiley Online Library (wileyonlinelibrary.com)

It is well known that hydrodynamics observed in large scale gas–solid fluidized beds are different from those observed in smaller scale beds. In this article, an efficient two-fluid model based on kinetic theory of granular flow is applied, with the goal to highlight and investigate hydrodynamics differences between three-dimensional fluidized beds of diameter 0.10, 0.15, 0.30, 0.60, and 1.0 m, focusing on the bubble and solids flow characteristics in the bubbling regime. Results for the 0.30 m diameter bed are compared with experimental results from the literature. The bubble size evolution closely follows a correlation proposed by Werther for small beds, and a correlation proposed by Darton for sufficiently large beds. The bubble size increases as the bed diameter is increased from 0.10 to 0.30 m, and remains approximately constant for bed diameters from 0.30 to 1.0 m. Concurrently, an increase in bubble rise velocity is observed, with a much high bubble rise velocity in the largest bed of diameter 1.0 m due to gulf stream circulations. The dynamics in shallow and deep beds is predicted to be different, with marked differences in bubble size and solids circulation patterns. © 2015 American Institute of Chemical Engineers *AIChE J*, 61: 1492–1506, 2015
Keywords: fluidized bed, two-fluid model, bed diameter, bubbles, solids motion

Introduction

The hydrodynamic behavior of gas–solid fluidized beds (FBs) is complex, difficult to understand, and remains an active area of research, in particular for large scale FBs. Processes can behave in a totally unpredicted manner if the influence of the complex hydrodynamics is ignored in these reactors. This not only reduces the efficiency of the process but can also lead to an economically unviable operation of the reactor. Therefore, a proper understanding of the hydrodynamics of FBs is essential to improve the performance and to achieve a rational scale-up to a commercial scale FB. Conversely, lack of understanding of the fundamentals of dense gas–particle flows in general has led to several difficulties in the design and scale-up of these reactors.[1] Difficulties can be associated with operating conditions and/or reactor dimensions. Information from a small scale reactor is used to predict the hydrodynamics in a larger scale reactor. However, failure has been reported[2] with this principle, as flow structures in large scale reactors are quite different from those observed in small scale reactors. Primarily, this is caused by wall-effects which are more dominant in small scale reactors than in large scale reactors. Solids circulation, gas flow and gas–solids contacting patterns in large reactors are different from those in small scale.[3] In small scale reactors, solids move upwards in the wakes of bubbles, while for industrial scale reactors more complicated toroidal gulf stream circulations, upflow in the center and downflow near the walls, are dominant.[4,5] The bubbles are primarily responsible for improved gas–solid contact and consequently the chemical conversion in a FB reactor. Unfortunately, the bubble size, the bubble frequency, and the bubble rise velocity are all strongly influenced by the bed size. In smaller beds bubbles move in the form of slugs, particularly at higher inlet gas velocities, whereas in larger beds bubbles grow in size due to coalescence. Because of the decreased wall effect in large scale FBs, bubbles move faster, resulting in less exchange with the dense phase.[6] These differences in the bubble behavior directly affect the contacting between gas and solids, and hence affect the chemical conversion. Furthermore, the hydrodynamics is expected to change when one moves from a very deep bed to a very shallow bed. A shallow bed at fixed inlet gas velocity shows a spontaneous oscillation of the free surface, and bubbles in a shallow bed have no room to develop on their way to the free surface.[7]

Many studies[8,9] are available on the effect of column diameter on the hydrodynamics of a bubble column. To some extent, the bubble behavior in a FB can be interpreted by analogy, but the bubble behavior in a solid bed is even more complex. Therefore, it is essential to know and understand the changes in hydrodynamic behavior in a gas–solids FB, when scaling up from very small to very large scale, and when changing the depth of a bed from very shallow to very deep.

Werther[10] suggested a minimum laboratory bed diameter of 0.50 m to conserve similar bubble characteristics related

Correspondence concerning this article should be addressed to J. T. Padding at j.t.padding@tue.nl.

to hydrodynamics, solids distribution, heat and mass transfer. Glicksman and McAndrews[11] found that the bubble rise velocity increases and the bubble chord length and bubble frequency decrease with bed diameter up to 0.6 m for FBs with relatively large particles. Particles from different classes show different flow behavior in different size reactors. Group A particles can achieve a condition where the rate of bubble growth equals the rate of breakup for relatively low gas velocity. So the average bubble size remains constant when the maximum stable bubble size is reached. In contrast, bubbles grow too much larger size for Group B particles than for Group A particles. Bubbling FBs are widely used in industry, due to their excellent heat and mass transfer characteristics and solids mobility required for efficient catalyst regeneration. The hydrodynamics of a bubbling FB is even more complex and known to change rapidly with change in bed diameter. Scaling laws have been developed by many researchers[12–15] to scale parameters, such as pressure drop and solids holdup, with bed diameter. Knowlton et al.[13] mentioned that with increasing bed diameter, there is a leveling off of the rate of change of the scaling to a constant value. The bed diameter at which this leveling off occurs is different for different particle classifications. For Geldart B type particles the leveling off occurs at larger bed sizes compared to Geldart A type particles. Recently, a critical review on scale up of bubbling FB has been presented by Rüdisülia et al.[15]

Almost all studies available in the literature[11,16] on the effect of bed diameter and scale-up are concerned with experimental and/or theoretical observations. Most experimental works conclude with a recommendation for numerical simulations to obtain detailed understanding of the experimental observations and the proposed scaling laws. To our knowledge, no numerical study on the effect of bed diameter on the hydrodynamics of a full three-dimensional (3-D) FB has been done, possibly due to the high computational costs. Fortunately, with increasing computational power such numerical simulations have become possible. In this work, we present two-fluid model (TFM) simulations, based on the kinetic theory of granular flow (KTGF), of bubbling fluidization for Geldart B particles in a cylindrical FB with diameters of 0.10, 0.15, 0.30, 0.60, and 1.0 m, respectively. We first show the reliability of the model by comparing results for a 0.30 m bed with experimental measurement of Laverman et al.[17] We calculate the bubble size by different possible approaches, and propose the most reliable approach. Then, we quantify the effect of bed size on the bubble size, the bubble aspect ratio, the bubble rise velocity, porosity distribution and solids velocity, and solids flow pattern. We also highlight the hydrodynamic differences between very shallow beds and deep beds.

This article is organized as follows. First a short description of the TFM is given, focusing on the main governing equations. Details on postprocessing of simulation data, to calculate bubble properties, are given. Subsequently, the results are presented, including details of the simulation settings, validation, and a discussion of the results. We finish with our conclusions.

Two-Fluid Model

The two-fluid continuum model describes both the gas phase and the solids phase as fully interpenetrating continua using a generalized form of the Navier–Stokes equations.[18,19] To describe the solids phase rheology, the KTGF[20,21] is used. The conservation equations are given in Tables 1 and 2. Here, the subscripts g and s represent the gas and solids phase, respectively. Details of the TFM used in this work, and the approach to efficient numerical solution in cylindrical coordinates, have been reported in Verma et al.[22] In our previous work,[23] we have presented a thorough validation of our TFM by comparing the bubble characteristics in a 0.10 m diameter bed for different granular materials and comparing with experimental X-ray tomography results.

Table 1. TFM Governing Equations

Continuity equation:	(T1–1)
$\frac{\partial(\varepsilon_g\rho_g)}{\partial t}+\nabla\cdot\left(\varepsilon_g\rho_g\bar{u}_g\right)=0$	
$\frac{\partial(\varepsilon_s\rho_s)}{\partial t}+\nabla\cdot(\varepsilon_s\rho_s\bar{u}_s)=0$	
Momentum equation:	(T1–2)
$\frac{\partial(\varepsilon_g\rho_g\bar{u}_g)}{\partial t}+\nabla\cdot\left(\varepsilon_g\rho_g\bar{u}_g\bar{u}_g\right)=$ $-\varepsilon_g\nabla p_g-\nabla\cdot\left(\varepsilon_g\bar{\bar{\tau}}_g\right)-\beta\left(\bar{u}_g-\bar{u}_s\right)+\varepsilon_g\rho_g\bar{g}$	
$\frac{\partial(\varepsilon_s\rho_s\bar{u}_s)}{\partial t}+\nabla\cdot(\varepsilon_s\rho_s\bar{u}_s\bar{u}_s)=$ $-\varepsilon_s\nabla p_g-\nabla p_s-\nabla\cdot(\varepsilon_s\bar{\bar{\tau}}_s)+\beta\left(\bar{u}_g-\bar{u}_s\right)+\varepsilon_s\rho_s\bar{g}$	
Granular temperature equation:	(T1–3)
$\frac{3}{2}\left[\frac{\partial}{\partial t}(\varepsilon_s\rho_s\Theta)+\ \nabla\cdot(\varepsilon_s\rho_s\Theta\bar{u}_s)\right]=$ $-\left(p_s\bar{\bar{I}}+\varepsilon_s\bar{\bar{\tau}}_s\right):\nabla\bar{u}_s-\nabla\cdot(\varepsilon_s q_s)-3\beta\Theta-\gamma$	

Post-Processing of Simulation Data

Postprocessing of 3-D simulation data is crucial when it comes to calculating bubble properties, in particular for the bubble size and the bubble rise velocity. For instance, the bubble may not remain spherical or even regular in shape and the bubble velocity may not be effectively in the direction of flow in a large FB. Not only the bubble size and velocity but also other parameters such as the bubble aspect ratio, porosity distribution, solids velocity and solids circulation patterns are equally important to quantify the fluidization characteristics. Therefore, before moving on to a detailed discussion of the results, in the following we present our approach to calculate the bubble and solids properties.

Bubble size

To calculate the bubble characteristics, information on the gas volume fraction (porosity), available for each computational cell in the domain of interest, is used. A threshold porosity value in the range of 0.70–0.75 can be used to define the bubble boundary, as justified in our previous work.[23] In this work, we have made the choice to designate cells with a porosity larger than 0.75 as bubble cells. A sophisticated technique of creating a cell list for individual bubbles has been developed, and a linear interpolation of porosities is used to calculate the precise location of the bubble boundary in the sharp gradient between bubble and emulsion phase. Note that most experimental measurements of 3-D bubbles in FBs are actually pseudo-two dimensional measurements, either in a vertical plane (intrusive probes) or in a horizontal plane (tomographic measurements). The bubble size correlations available in the literature are obtained from such measurements. These measurements techniques are quite fair for small bed sizes, where small and regularly shaped bubbles are observed, which are symmetric in either

Table 2. KTGF Closures for TFM

Particle pressure: $p_s = [1+2(1+e_n)\varepsilon_s g_0]\varepsilon_s \rho_s \Theta$	(T2-1)
Bulk viscosity: $\lambda_s = \frac{4}{3}\varepsilon_s \rho_s d_p g_o (1+e_n)\sqrt{\frac{\Theta}{\pi}}$	(T2-2)
Shear viscosity: $\mu_s = 1.01600\frac{5}{96}\pi\rho_s d_p \sqrt{\frac{\Theta}{\pi}}\frac{(1+\frac{8}{5}\frac{(1+e_n)}{2}\varepsilon_s g_0)(1+\frac{8}{5}\varepsilon_s g_0)}{\varepsilon_s g_0} + \frac{4}{5}\varepsilon_s \rho_s d_p g_0 (1+e_n)\sqrt{\frac{\Theta}{\pi}}$	(T2–3)
Dissipation of granular energy due to inelastic particle–particle collision: $\gamma = 3(1-e_n^2)\varepsilon_s^2 \rho_s g_0 \Theta\left[\frac{4}{d_p}\sqrt{\frac{\Theta}{\pi}} - (\nabla \cdot \vec{u}_s)\right]$	(T2–4)
Pseudo-Fourier fluctuating kinetic energy flux: $\vec{q}_s = -\kappa_s \nabla\Theta$	(T2–5)
Pseudo thermal conductivity: $\kappa_s = 1.02513\frac{75}{384}\pi\rho_s d_p \sqrt{\frac{\Theta}{\pi}}\frac{(1+\frac{12}{5}\frac{(1+e_n)}{2}\varepsilon_s g_0)(1+\frac{12}{5}\varepsilon_s g_0)}{\varepsilon_s g_0} + 2\varepsilon_s \rho_s d_p g_0 (1+e_n)\sqrt{\frac{\Theta}{\pi}}$	(T2- 6)

of the measurement planes. However, for larger bed sizes irregular bubble shapes are observed. Levenspiel[24] pointed out the problem of scale-up due to the difficulty of estimating a reasonable bubble size for frantically changing shapes of bubbles in large beds. Perhaps this is an advantage for simulations: one can obtain as detailed information as desired. Therefore, to make a fair comparison of bubbles in different bed sizes and also with literature correlations, we present the bubble size as calculated from three possible approaches. The three definitions of equivalent bubble diameter, given in Eqs. 1, 2, and 3, respectively, are pictorially shown in Figure 1. In Eq. 1, a cross-sectional plane in the r-θ direction (horizontal plane) at a specified height is considered. This approach of calculating the equivalent bubble diameter is similar to experimental measurements from tomographic techniques,[23–27] where scanning of a 3-D FB is performed instantaneously in 2-D cross-sectional planes. We should note that researchers[25,28] have obtained pseudo-3-D images of the bubbles, by using the time scale, indicating bubble motion, in the third direction. This may lead to inconsistencies on the bubble size because the time dependent process (the bubble rise velocity) is highly dependent on the bubble size. So to test the reliability of this approach it is worthwhile to investigate results obtained from a similar approach. The second approach is to calculate the bubble size from Eq. 2, where a cross sectional plane in the r-z direction (vertical plane) through the center of the 3-D bed is considered. This approach is similar to intrusive probe measurements to obtain the bubble pierced length, where the signal of the rising bubble piercing the probes is recorded to estimate their vertical size and motion. It is well know that bubbles are nonuniformly distributed in 3-D FBs. Therefore, the bubble pierced length may not represent the actual bubble diameter. Although semiempirical correlations are fitted for lateral motion of the bubble by measuring signals at different lateral positions in 3-D FBs, these are independent measurements, considering signal variation at one fixed location at a time. Nevertheless this approach of measurements seems to be more reliable, when measuring bubbles in different bed diameters. The most realistic approaches consider the full 3-D volume of the bubble to obtain the equivalent bubble diameter. Very advanced experimental techniques are required to calculate the actual 3-D bubble volume, such as volumetric tomography at very high spatial resolution. These techniques are very costly and not easy to develop. However, simulations have a natural advantage to follow this approach: we track individual 3-D bubble volumes and calculate the equivalent bubble size, equivalent meaning based on a spherical bubble of equal volume (Eq. 3). Information on the bubble expansion in the lateral and/or in the axial direction can be obtained from the bubble aspect ratio (Eq. 4), defined as the ratio of maximum vertical length of the bubble to the maximum horizontal length.

The number of predicted bubbles is used to obtain the averaged equivalent bubble diameter. In this work, the predicted equivalent bubble diameter is compared with the correlations of Darton et al.[29] and Werther.[30] Expressions for these correlations are given in Table 3

$$D_{eH} = \sqrt{\frac{4A_{r-\theta}}{\pi}} \tag{1}$$

$$D_{eV} = (z_{\max} - z_{\min})_{r-z} \tag{2}$$

$$D_{e3\text{-D}} = \sqrt[3]{\frac{6V}{\pi}} \tag{3}$$

$$\text{AR} = \frac{Z_{\max} - Z_{\min}}{X_{\max} - X_{\min}} \tag{4}$$

Porosity distribution

The porosity distribution function (PDF) quantifies the relative occurrence of porosities in the emulsion phase and the bubble phase. To obtain the PDF a small porosity bin size of 0.01 is used, and the variable cell size in the computational cylindrical domain is properly taken into account.

Bubble velocity

For most experimental measurement in the literature,[23,31,32] the bubble rise velocity is calculated by cross-correlating a bubble signal captured at two different locations, separated by a small vertical distance. For a proper comparison, we have also calculated the bubble rise velocity from a cross-correlation function (CCF) of the porosity values in r-θ planes separated by a vertical distance of 15 mm. Details of calculating this CCF have been reported in our previous work.[23] Another approach to calculate the bubble rise velocity is by using a "bubble tracking method," considering

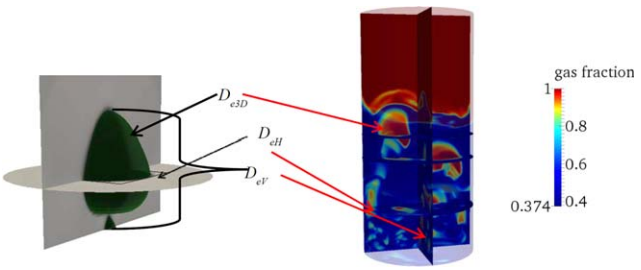

Figure 1. Pictorial representation of the definition of three different bubble diameters on a single isolated bubble and showing planes of measurement in the 3-D FB.

[Color figure can be viewed in the online issue, which is available at wileyonlinelibrary.com.]

Table 3. Equivalent Bubble Size Correlations Compared in This Work

Author(s)	Correlation	U_0- U_{mf} (m/s)	Bed Size (m)
Darton et al.	$D_e=0.54\left(U_0-U_{mf}\right)^{0.4}\left(H+4\sqrt{A_0}\right)^{0.8}g^{-0.2}$	0.005–0.20	0.30 × 0.30 0.30 × 0.20 0.61 × 0.61 1.0
Werther	$D_e=d_0\left[1+27\left(U_0-U_{mf}\right)\right]^{1/3(1+6.4H)^{1.21}}$	0.05–0.30	0.45 1.0
		Geldart B, $d_0 = 0.00853$ m	

individual bubble motion. In this approach, the displacement of the centroid of each bubble is traced. The net movement of the centroid of a bubble with time provides the bubble rise velocity. We have compared the predicted bubble rise velocity with the correlation of Hilligardt and Werther,[33] which is given in Table 4.

Solids motion

The solids motion in the 3-D bed is averaged azimuthally and time-averaged to emphasize the average motion of solids from the center to the wall. Note that in our plots not all vectors will be shown to avoid close overlapping vectors and to maintain clarity of the plots.

Results and Discussion

In this work, the choice of bed material and operating conditions corresponds to those of the experimental measurements by Laveraman et al.[17] They performed experiments using positron emission particle tracking on a bed of diameter 0.306 m, using different granular materials and different superficial gas velocities. Specifically, we will focus on linear low density polyethylene (LLDPE) particles at an inlet gas velocity of $2.5U_{mf}$. This will allow us to compare our simulation results with experimental measurements for a specific bed diameter, after which we will study scale-up effects by varying the bed diameter. Details on the TFM simulation settings can be found in Table 5. The FB dimensions, with details of the computational grid size, are presented in Table 6. We performed simulations for a total time of 10.0 s. Time-averaging was performed by ignoring the initial first second to avoid inclusion of start-up effects. The quasi-steady state is identified when the time-averaged solids circulation patterns have become steady.

Grid independence, drag force comparison, and experimental validation

Before investigating the effect of bed diameter on bubble and solids flow characteristics, we will show the grid size independence, drag force correlation, and experimental validation for a bed of diameter 0.30 m. It is known that numerical solutions are grid dependent, where solutions obtained on too coarse grids might not be accurate. Refined grid simulations are required to obtain accurate solutions. At the same time, simulations on too fine grids require very small time-steps, which simply makes them computationally too expensive for large 3-D FBs. The proper choice of grid size should be such that it resolves gas–solids flow structures on the smallest relevant microscopic length and time scales. In our previous study,[22] we showed that the number of grid cells in the azimuthal direction does not have a significant effect; 24 to 30 cells in the azimuthal direction is sufficient to obtain a grid independent solution. Therefore, in this work, we take a fixed value of 30 cells in the azimuthal direction and test the grid dependence in the radial and axial directions. Simulation results obtained using grid sizes of 3.4 and 5.0 mm (with an equal grid size in radial and axial direction for both cases) are compared. Figure 2a shows that the bubble size predicted using a grid size of 5.0 mm is slightly larger than for a 3.4 mm grid, and proportionally the bubble rise velocity is slightly larger (see Figure 2b). This is caused by the fact that bubbles smaller than 5.0 mm cannot be resolved on a grid of 5.0 mm. Figure 3 shows the azimuthally and time-averaged solids circulation pattern, comparing experiment and simulation. The simulation results show close agreement with experimental findings, with small differences in the lower vortex configuration, which is clear in the simulation and diminished in the experiments. The small differences between simulation and experimental results can be attributed to the particle size distribution in the experiments. Figure 4a shows the azimuthally and time-averaged axial solids velocity profile at three different height. The simulation results show close agreement with the experimental observations for the grid size of 3.4 mm. However, simulation on such refined grids becomes computationally too expensive for larger beds. Therefore, to reduce the computational efforts we have chosen to use the 5 mm grid size in radial and axial directions. The results on bubble diameter, bubble velocity and solids velocity do not show a significant difference for these two different grid sizes.

Gas–particle drag plays an important role in FB reactors. In literature, many studies are available comparing different drag force models. However, almost all are limited to 2-D systems. Therefore, in this study, we compare drag model from Ergun[37]/Wen and Yu[36] and the drag model of Van der Hoef et al.[34] Figure 4b shows results obtained with both models for a grid size of 3.4 mm, along with experimental

Table 4. Literature Correlation for Bubble Velocity for Geldart B Type Particles

Author(s)	Correlation	U_0- U_{mf} (m/s)	Bed Size (m)
Hilligardt and Werther	$u_b=0.2\sqrt{D}0.71\sqrt{gD_e}+\psi\left(U_0-U_{mf}\right)$ $\psi=\begin{cases}0.67 & \mathrm{AR}<1.7\\ 0.51\sqrt{\mathrm{AR}} & 1.7\le\mathrm{AR}\le 4\\ 1 & \mathrm{AR}>4\end{cases}$	0.05–0.30	0.30 × 2.0 0.50 × 0.50 1.0 × 1.0

Table 5. TFM Simulation Settings

Particle density	800 kg/m^3
Particle diameter	1.1 mm
Coefficient of restitution	0.69
Initial solids volume fraction	0.6
Minimum fluidizing velocity (U_{mf})	0.26 m/s
Superficial gas velocity	2.5U_{mf}
Gas–particle drag	Van der Hoef et al.[34]
Frictional stress model	Srivastava et al.[35]
Flow solver time-step	10^{-4} s
Total simulation time	10.0 s

results from Laverman et al.[17] We choose to compare the different drag models for the finer grid to emphasize that even for a fine enough grid the simulation results are sensitive of the drag model used. The simulation results show close agreement with the experimental observations when drag model from Van der Hoef et al.[34] is used. Superiority of Van der Hoef et al.[34]model over other drag models has previously been reported by Bokkers[38] for single bubble injection in a FB. Therefore, in this study, we used drag force model from Van der Hoef et al.[34] Note that for larger grid sizes it becomes increasingly important to take into account the effect of formation of subgrid scale structures on the effective gas–solid drag. This has been modelled by Sundaresan and coworkers[39,40] as an adapted drag force, including terms which depend on the local solid volume fraction and the so-called filter size.

General bubble characteristics

Figure 5 shows instantaneous 3-D bubble contours for different bed diameters. This figure clearly shows that small beds have bubbles with a regular shape in the bottom section of the bed, and elongated bubbles in the top section of the bed. Moving toward larger beds, the bubbles become more chaotic and randomly shaped. Mostly bubbles are initiated near the wall and move toward the center of the bed, driven by the lower resistance offered in the center. We also observe that in the largest beds, specifically for bed diameters 0.6 and 1.0 m, significantly many lenticular (pancake shape) bubbles are initiated from the bottom (see Figures 5c–e). These lenticular bubbles change to regular bubbles within a few centimeters height. References 41, 42 also mention formation of these lenticular shape cavities at the bottom. They also mention that these cavities rise with great difficulty because of its bluff shape and the viscous nature of the bed. At a height of 5 to 6 cm these lenticular cavities split into smaller regular bubbles. In our simulations, these phenomena are predominantly predicted for the larger beds.

Figure 6 shows the azimuthally and time-averaged porosity plots. The porosity at the center is higher for a smaller bed and gradually decreases for larger beds, specifically in the bottom section of the bed. The region of higher average

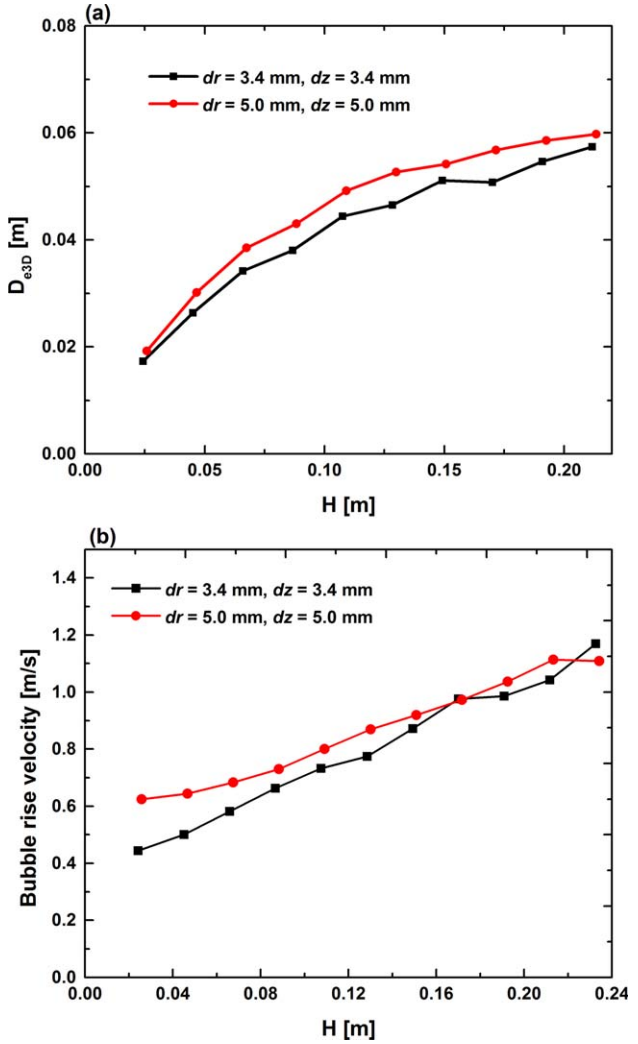

Figure 2. Effect of the grid size on (a) the equivalent bubble diameter, and (b) the bubble rise velocity, at different height from the bottom in the bed diameter of 0.30 m.

[Color figure can be viewed in the online issue, which is available at wileyonlinelibrary.com.]

porosity is the bubble active zone, which intensifies and moves toward the center with increasing height. These plots reveal the preferred path of bubbles through the bed. At the distributor, for bed diameters of 0.10, 0.15, and 0.30 m, the bubbles prefer to form at $r/R = 0.8$, while for bed diameters of 0.60 and 1.0 m, the bubbles prefer to form at r/R close to 1.0 and reach the center of the bed ($r/R = 0$) at a height approximately equal to the bed diameter. Stefanova et al.[43] also observed the highest time-average local voidage at $r/R = 0$ for a 0.29 m diameter bed and at $r/R = 0.6$ for a

Table 6. Computational Parameters and Bed Size Specifications

Property	Case 1	Case 2	Case 3	Case 4	Case 5	Case 6
Bed diameter (m)	0.10	0.15	0.30	0.60	1.00	1.0/2.0
Overall height of the domain (m)	0.50	0.60	0.60	1.25	1.75	0.40
Initial particle bed height (m)	0.30	0.30	0.30	0.60	1.00	0.10
Number of grids in r-direction (nr)	10	15	30	60	100	100/200
Number of grids in θ-direction ($n\theta$)	30	30	30	30	30	30
Number of grids in z-direction (nz)	100	120	120	250	350	80

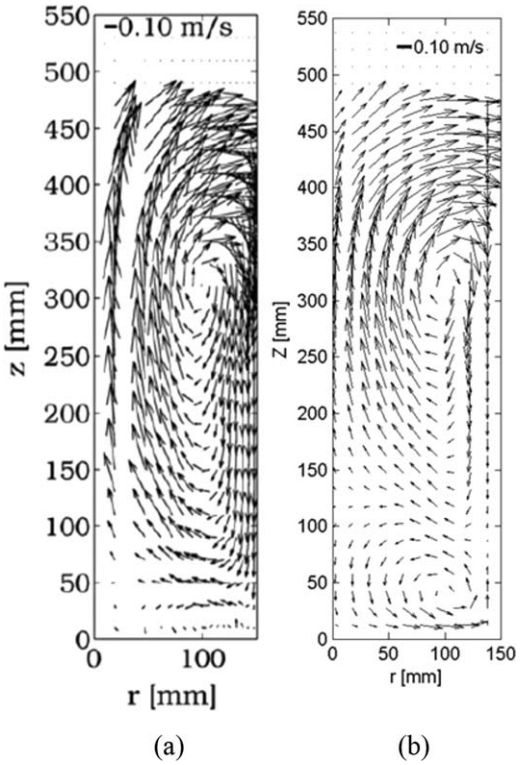

Figure 3. Azimuthally and time-averaged solids circulation in the bed diameter of 0.30 m, obtained from (a) experiment; Laverman et al.[17] and (b) simulation. For clarity only every third vector in the radial and axial direction is shown.

1.56 m diameter bed, when measured at a height of 0.47 and 0.6 m, respectively. For the bed diameter of 0.10 m, above a height of approximately twice the bed diameter the high time-averaged porosity reveals that bubbles are moving in the form of slugs. The round nose of a slug bubble is observed in the 3-D bubble contours seen in Figure 5a. This round nose shape indicates smooth slugging.[42] In such a slugging bed, the solid flows past the slug in an annulus region near the wall. This is dominant for a bed diameter of 0.1 m because of the sufficiently deep bed compared to the bed diameter.

A local solids holdup is observed for all bed diameters in the time-averaged porosity plot in Figure 6 at $H/h_0 = 1$ near the wall. This region is the least active bubble zone and is created due to eruption of bubbles into the freeboard region and flashing of particles toward the wall. The width of this heap increases with increase in bed diameter, revealing that bubbles erupt mostly from the center of the bed. Figure 6 also shows that the high particle shear zone ($\varepsilon_g < 0.5$) in the center becomes dominant when the bed size is increased from 0.15 to 1.0 m. This shows that rising voids follow a nearly perfect annulus trajectory, with solids holdup in the bottom center and near the wall at the top. Very similar trends in porosity gradient are predicted for bed diameters of 0.1 to 0.6 m. However, small differences for the bed diameter of 1.0 m are seen, where the porosity is more widely spread in the top section of the bed, with a lower porosity region near the center at $H/h_0 = 1$. This shows that bubbles in a 1.0 m diameter bed tend to not erupt in the center, or that the bubbles do not reach the center as they travel from the bottom. At this stage, the argument could be that the bubble size variation with axial and lateral position is different in a bed of 1.0 m. We will return to this point later.

Figure 7 shows the PDF for different bed diameters, for a height between 0.15 and 0.30 m from the bottom. The PDF plots shows that bubble (high porosity) holdup is higher for smaller beds and decreases for larger beds. This is consistent with the observations reported by Volk et al.[44] and by Werther.[16] A higher bubble holdup, in smaller beds of 0.1 and 0.15 m, is the cause of continuous chains of rising bubbles in the center and less emulsion/dense phase surrounding them. A decreasing trend in bubble holdup and an increasing amount of denser phase is predicted when the bed diameter is increased further from 0.30 to 1.0 m. Effectively this decrease in bubble holdup with increase in bed size may result in a decrease in mass transfer area, hence the chemical conversion is altered.[16]

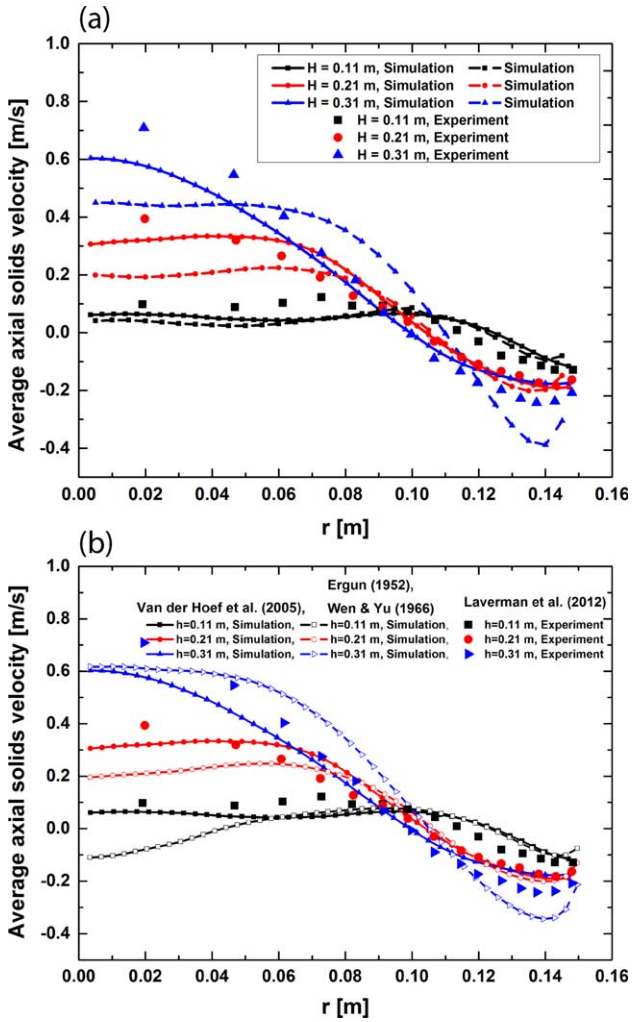

Figure 4. Azimuthally and time-averaged axial solids velocity at three different height in the bed diameter of 0.30 m, comparing experiments and simulations.

(a) Effect of different grids size. Solid lines represent simulation on grids size of 3.4 mm and dashed lines represent simulations on 5.0 mm grid size in radial and axial direction respectively. (b) Effect of different drag force models. Line with solids symbols: Van der Hoef et al.[34], line with open symbols: Ergun[37]/Wen and Yu[36]. [Color figure can be viewed in the online issue, which is available at wileyonlinelibrary.com.]

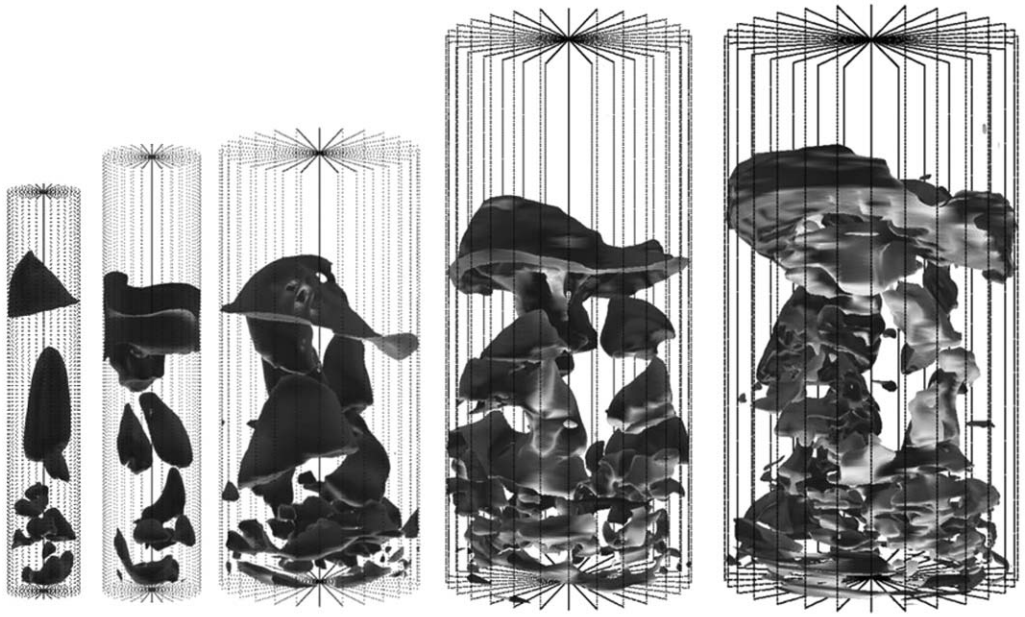

Figure 5. 3-D bubble iso-surfaces ($\varepsilon_g = 0.75$) for a bed diameter of (a) 0.10, (b) 0.15, (c) 0.30, (d) 0.60, and (e) 1.0 m diameter.

Note that these images are not to (relative) scale. Actual dimensions of the beds are given in Table 6.

Bubble size

The bubble size is the most important factor in the design and scale-up of FBs. In the literature, a very mixed understanding of the bubble size is available, particularly for Geldart B particles in bubbling FBs. Many different correlations are available. The best known are from Darton et al.[29] and Werther.[30] The Darton correlation is based on capacitance probe measurement and X-ray photography in beds with a diameter in the range of 0.30–1.0 m, whereas the Werther correlation is based on capacitance probe measurements in beds with a diameter in the range of 0.45–1.0 m. Both these correlations are dependent on excess gas velocity and height from the bottom, but do not take into account the bed diameter explicitly. Rather, the authors[29,30] developed these correlations by collecting data obtained from different bed sizes. We will compare the bubble sizes predicted for different bed diameters with these two correlations. For the Darton correlation, the initial bubble size A_0 was set to zero, assuming zero bubble size at zero height. The bubble size increases

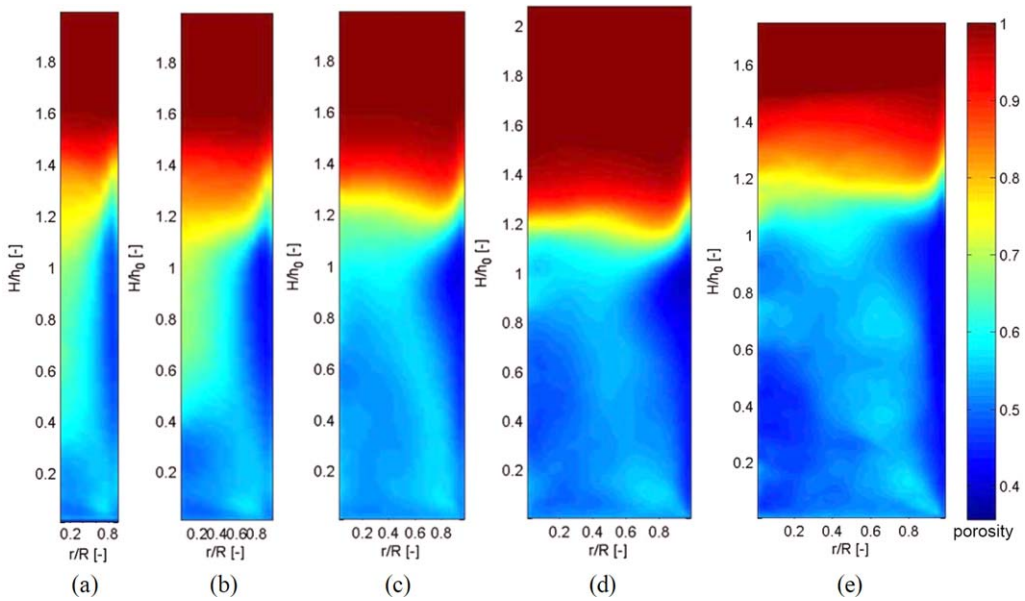

Figure 6. Azimuthally and time-averaged porosity plot in a bed diameter of (a) 0.10, (b) 0.15, (c) 0.30, (d) 0.60, and (e) 1.0 m.

Initial particle bed height (h0) for (a–c) is 0.30 m, for (d) is 0.60 m, and for (e) is 1.0 m. [Color figure can be viewed in the online issue, which is available at wileyonlinelibrary.com.]

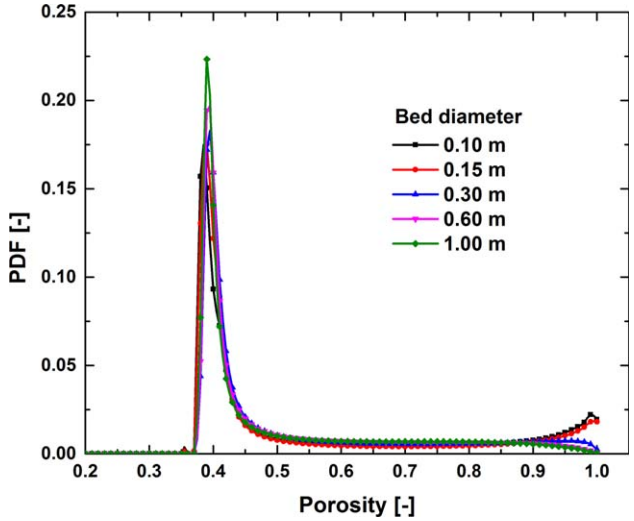

Figure 7. PDF plot for different bed diameter, between the height of 0.15–0.30 m from the bottom.

[Color figure can be viewed in the online issue, which is available at wileyonlinelibrary.com.]

with increasing height from the bottom, due to bubble coalescence and continuous gas extraction by the bubble from the emulsion phase. 3-D bubbles can coalesce either by merging of trailing bubbles or by moving sideways (in the horizontal direction) and incorporating nearby bubbles. Details on bubble properties predicted from simulations in different bed diameter are discussed in the following paragraphs.

Figure 8 shows a comparison of the three definitions of equivalent bubble diameter in the bed of diameter 1.0 m. From all three approaches, a monotonously increasing trend in the equivalent bubble diameter with height is observed. However, quantitatively different trends of bubble growth are predicted when considering 2-D planes and the 3-D volume of the

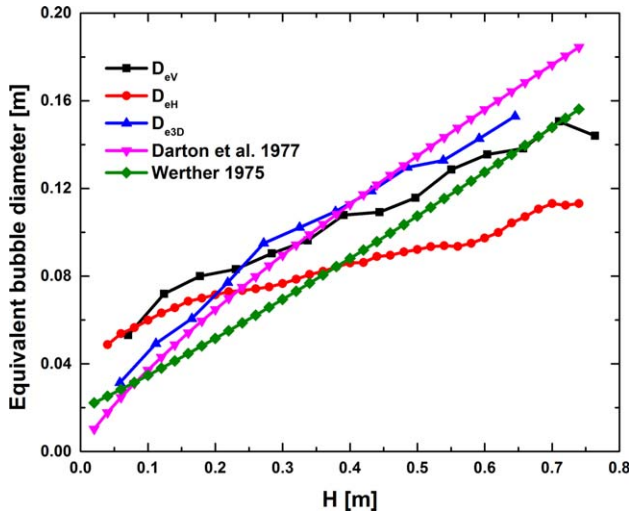

Figure 8. Comparing three different approaches of calculating the equivalent bubble diameter, as shown in Figure 1, in the bed diameter of 1.0 m as a function of height from the bottom.

[Color figure can be viewed in the online issue, which is available at wileyonlinelibrary.com.]

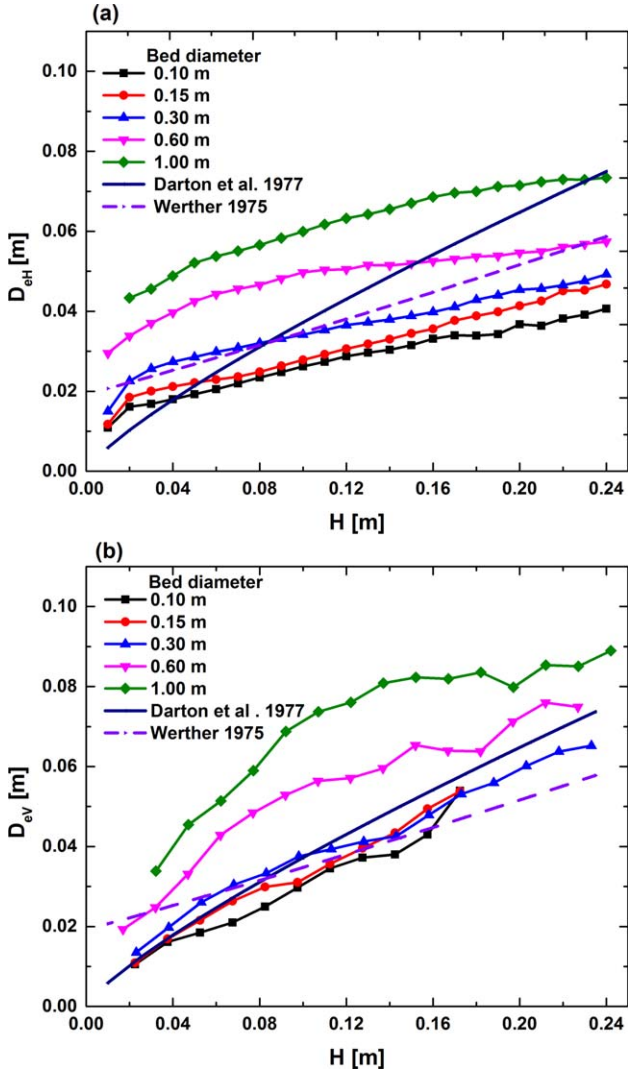

Figure 9. The average bubble diameter as a function of height calculated from (a) horizontal cross-sectional plane (Eq. 1) and (b) central vertical plane (Eq. 2), comparing different bed diameters and literature correlations.

[Color figure can be viewed in the online issue, which is available at wileyonlinelibrary.com.]

bubble. It is interesting to see that D_{eV} and D_{eH} effectively follow the Werther correlation, while $D_{e3\text{-}D}$ follows more closely the Darton correlation. This may be due to the fact that the Werther correlation is based on measurements of the bubble pierce length, which apparently follows the definition of D_{eV}. Glicksman and McAndrews[11] also confirmed the correlation between the mean vertical bubble chord length and the mean bubble diameter based on a log-normal distribution of the bubble size. Our results show that only the Darton correlation predicts a bubble size close to one obtained from the 3-D bubble volume for all axial positions. Recently, Karimipour and Pugsley[45] presented a critical review on the bubble size and the bubble velocity and found superiority of the Darton correlation to predict the actual bubble size. Our results clearly show that the precise approach of calculating the equivalent bubble diameter can make a profound difference on the obtained bubble size.

Figures 9a, b, and 10 show the equivalent bubble diameter calculated from horizontal (D_{eH}), vertical (D_{eV}) cross-sectional

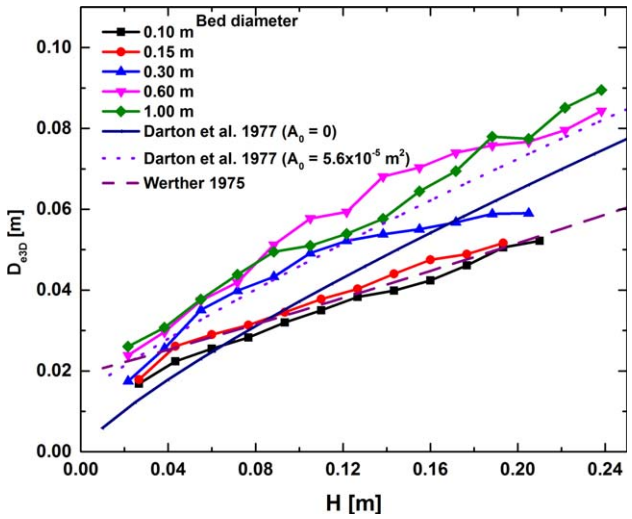

Figure 10. The average bubble diameter as a function of height, calculated from 3-D volume (Eq. 3) of the bubble, comparing in different bed diameters and literature correlations.

[Color figure can be viewed in the online issue, which is available at wileyonlinelibrary.com.]

planes and the bubble volume, respectively, for different bed diameters. These figures show an increase in bubble size when moving from smaller to larger beds. The figures also shows that for the bed diameter of 0.10 and 0.15 m the bubble size is nearly the same whether calculated horizontally, vertically, or from the 3-D bubble volume. This can intuitively be expected if the bubbles are spherical and regular in shape. Figures 9a, b shows a considerable increase in D_{eV} and D_{eH} as the bed diameter is increased from 0.30 to 0.60 m and from 0.60 to 1.0 m respectively. However, Figure 10 shows a considerable increase in $D_{e3\text{-}D}$ only when the bed diameter is increased from 0.15 to 0.30 m. For bed diameters of 0.30, 0.60, and 1.0 m, $D_{e3\text{-}D}$ does not show a significant difference. This shows that bubble size is leveling off for a bed diameter in between 0.30 and 0.60 m. Werther[10] mentioned the leveling off in the bubble properties at a bed diameter of 0.5 m. Our simulation results show that this statement is true if the bubble size is determined from the bubble volume. Furthermore, other bubble properties studied in the following sections will reflect in detail the leveling off with increasing bed diameter. Figure 10 also shows that the bubble size predicted by the simulations are close to the Darton correlation if catchment factors in their correlation is taken into account. This might be caused by the fact that in our simulations bubbles less than 5 mm (one grid size) are ignored in the processing. At this stage, we can conclude that the Darton correlation shows a close agreement throughout the height for larger bed diameters. We suggest to use it with caution for smaller bed diameters. For the bed diameters of 0.1 and 0.15, the Werther correlation shows very good agreement.

Figure 11 shows the azimuthally and time-averaged bubble size as a function of dimensionless radial position, considering different sections of the bed. In the bed section from 1 to 15 cm (Figure 11a), the bubbles are larger at the central axis for bed diameters of 0.10, 0.15, and 0.30 m, while for bed diameters of 0.60 and 1.0 m larger bubbles are located in an annular region between the wall and the central axis. This is the reason why bubbles in larger bed have to

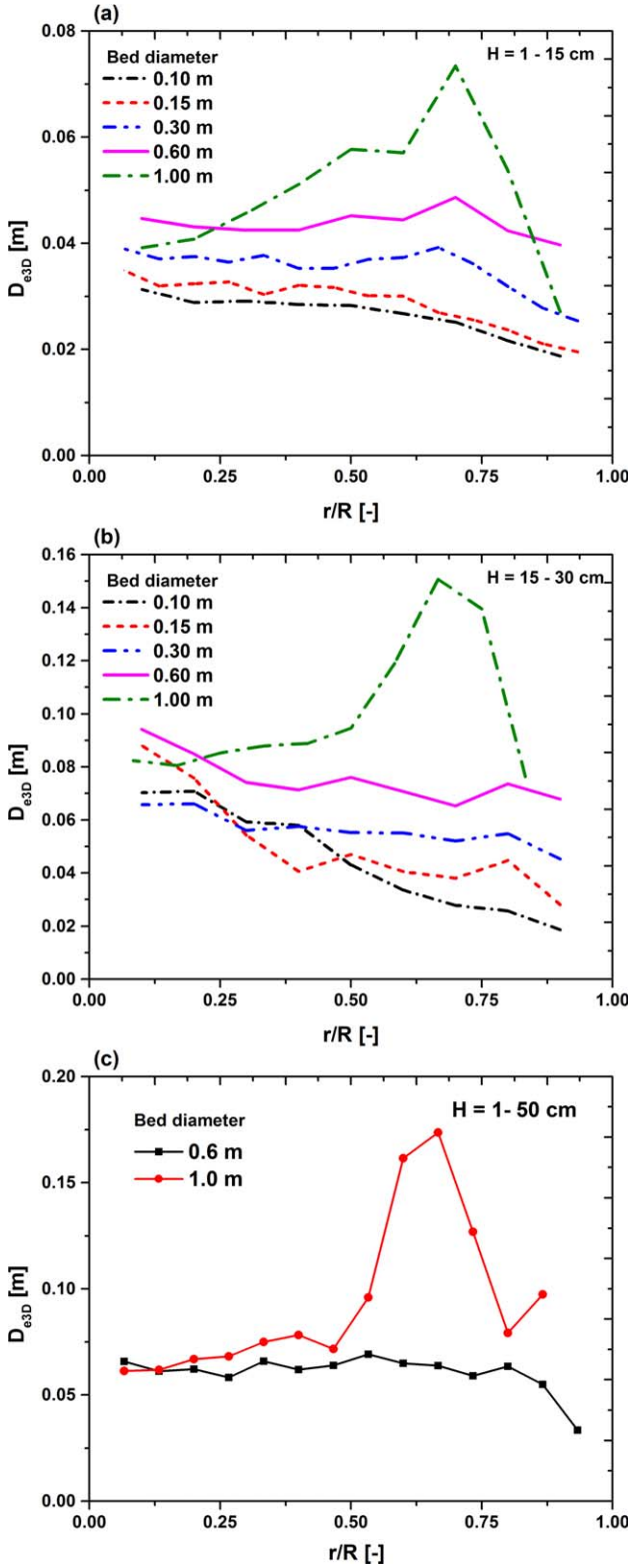

Figure 11. The average bubble diameter as a function of dimensionless radial position, averaged between a height of (a) 0.01–0.15 m and (b) 0.15–0.30 m and (c) for bed diameter of 0.6 and 1.0 averaged between 0.01 and 0.50 m from the bottom.

[Color figure can be viewed in the online issue, which is available at wileyonlinelibrary.com.]

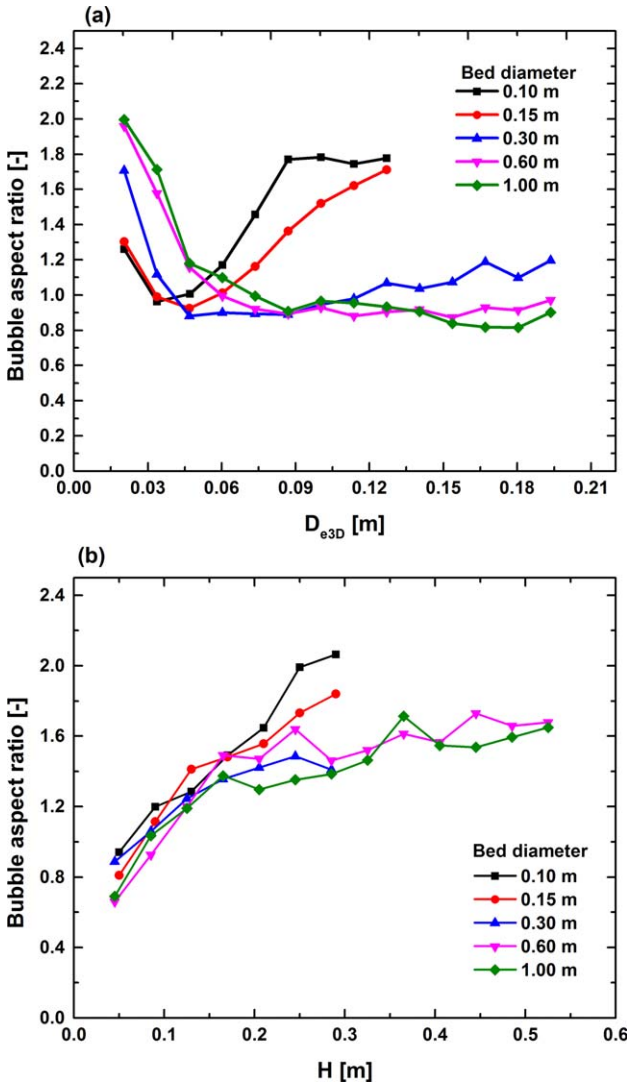

Figure 12. The bubble aspect ratio, comparing different bed diameters, as a function of (a) the bubble diameter and (b) the height from the bottom.

[Color figure can be viewed in the online issue, which is available at wileyonlinelibrary.com.]

move a long distance to reach the center. In the bed section from 15–30 cm (Figure 11b), the bubbles in the center are still smaller for a bed diameter of 1.0 m. Figure 11c compares the lateral variation of bubble size in the beds with a diameter of 0.6 and 1.0 m. The bubbles in the bed of 0.60 m diameter attain a nearly uniform distribution, whereas bubbles in the larger bed of 1.0 m diameter tend to be larger at a radial distance of about 2/3 of the bed radius. This shows that lateral variation of the bubble size is dependent on the bed diameter. The bubbles reach the center at a height approximately equal to the bed diameter.

The shape of the bubbles can be estimated from the bubble aspect ratio. Figure 12a shows the aspect ratio as a function of bubble size, for different bed diameters. A decreasing trend in bubble aspect ratio with increasing bubble size is predicted, until the bubble size equals half the bed diameter. When the bubble size becomes larger than half the bed diameter, the bubble starts to show vertical elongation. This is dominant in the smaller beds of 0.10 and 0.15 m diameter because larger bubbles in smaller beds are expected to move in the form of slugs. The bubbles aspect ratio observed in beds of diameter 0.60 and 1.0 m are nearly equal, both with flattened large bubbles. These larger bubbles show more lateral expansion due to diminished wall effects and more available space to expand in the radial direction.

Figure 12b shows changes in the bubble aspect ratio with the height from the bottom, revealing that the bubble aspect ratio decreases with increasing bed diameter. Flat bubbles are predicted in the bottom section, but with increasing height from the bottom the bubble aspect ratio increases for all beds sizes. The bubble aspect ratio is smaller in the largest bed, again revealing that bubbles have more space to expand in the radial direction as the bed diameter is increased. Glickman and McAndrews[11] made the same observation that the bubble chord length decreases with increasing bed diameter up to 0.6 m for large particle FBs. Figure 12b shows that above a height of 0.30 m, the bubble aspect ratio is nearly constant and equal to the average value of small and large bubble aspect ratios as projected from Figure 12a. This shows the existence of smaller and larger bubbles in the higher section of the bed, due to splitting of larger bubbles.

Overall, our analysis of bubble size shows that bubbles are initiated from the region near the wall and reach the center at a height equal to the bed diameter. The effective bubble size should be predicted taking into account 3-D bubble volume. In the smaller beds, bubbles are small and nearly spherical, and larger slugging bubbles are predicted above a height of twice the bed diameter. In the larger beds, bubbles are larger and predominantly of random shape. The bubbles expand more in the horizontal direction in larger beds. The bubbles predicted in bed diameters of 0.6 and 1.0 m show similar characteristics for the bubble size and bubble shape factor.

Bubble rise velocity

As mentioned in the postprocessing section, the bubble rise velocity can be obtained either from tracking individual bubbles, or by cross-correlation of porosity values between two horizontal cross-sectional planes separated by a vertical distance of 15 mm. Figure 13a shows the bubble rise velocity in a bed of 0.30 m comparing these two approaches. Both approaches predict nearly the same bubble rise velocity in a 0.30 m bed. When comparing the two approaches at a fixed height for different bed diameters, as in Figure 13b, the bubble rise velocity is indeed very similar for small beds but different for the larger bed diameters of 0.60 and 1.0 m. This may be caused by the fact that the bubble tracking method is biased toward smaller bubbles, which rise more slowly, and might not be accurate enough to predict the motion of very large bubbles, which rise fast. In general, due to the random motion of bubbles, particularly in very large beds, calculating the bubble rise velocity from bubble tracking methods becomes complicated in 3-D FBs, possibly leading to inaccurate results. Therefore, we believe that for a fair comparison between the bubble rise velocity in our simulations and the literature correlation,[33] the cross-correlation technique is the most accurate one. Furthermore, bubble rise velocity correlations available in the literature[32,33] have mostly been obtained from similar auto- and cross-correlation techniques. Therefore, from this point onwards,

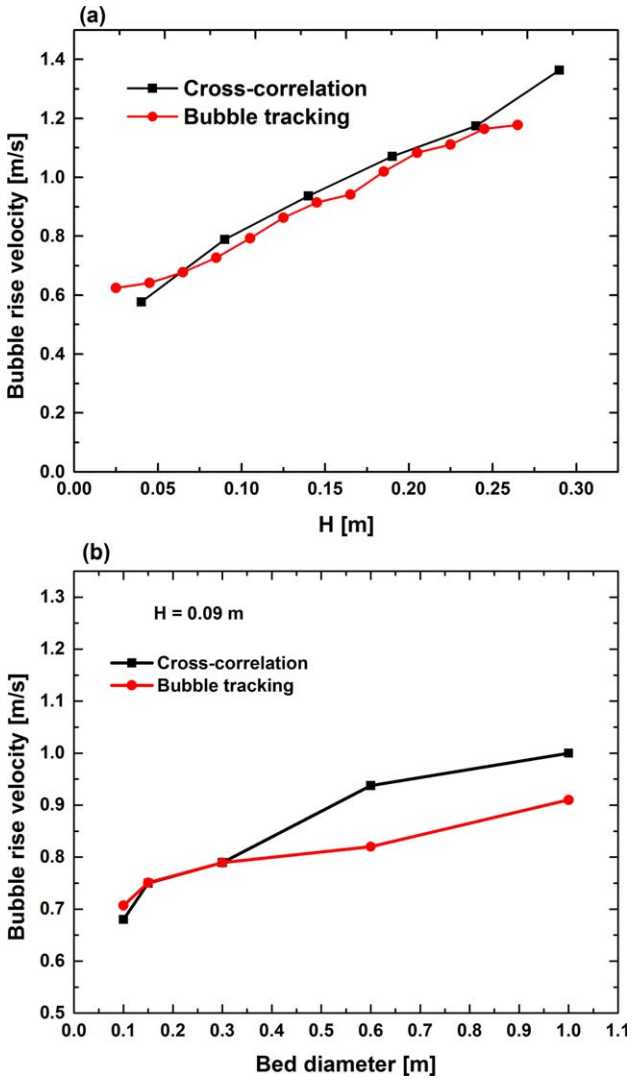

Figure 13. The bubble rise velocity calculated from cross-correlation and bubble tracking technique, (a) compared in the bed diameter of 0.30 m, and (b) compared for all bed size at fixed height of 0.09 m from the bottom.

[Color figure can be viewed in the online issue, which is available at wileyonlinelibrary.com.]

we will report bubble rise velocities calculated from the cross-correlation technique.

Figure 14 shows the bubble rise velocity as a function of height for different bed diameters. The bubble rise velocity increases with increasing bed diameter and with increasing bed height. This increase in bubble rise velocity with increase in bed size is due to increase in bubble size and diminishing wall effects. A notable increase in bubble rise velocity is predicted for a 1.0 m diameter bed, above a height of 0.15 m. This is due to the gulf streaming phenomenon, as discussed by Merry and Davidson.[46] The gulf streaming phenomenon is caused by nonuniform bubble flow in the cross sectional area, causing a general upward solids flow in one part of the bed, and downward in the other. Due to the large cross-sectional area available in a 1.0 m diameter bed, this phenomenon is dominant and resulting in a higher bubble rise velocity. The gulf stream pattern will be further discussed in detail in the later section when we compare solids circulation patterns.

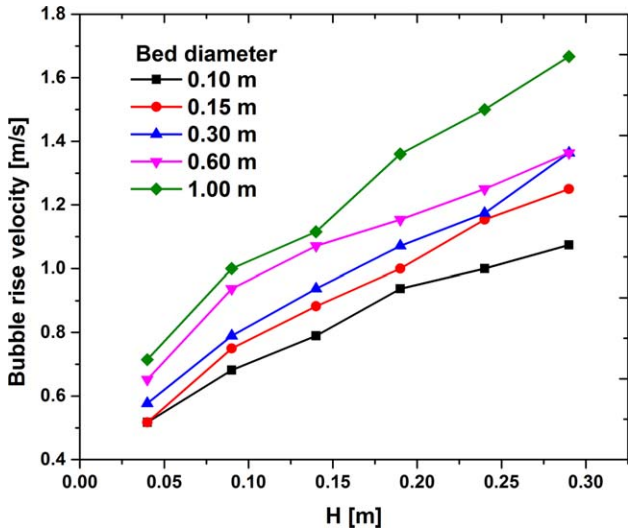

Figure 14. The bubble rise velocity as a function of height from the bottom, compared in different bed size.

[Color figure can be viewed in the online issue, which is available at wileyonlinelibrary.com.]

Figure 15a shows the bubble rise velocity for different bed diameters at fixed height of 0.09 m, together with the Hilligardt and Werther[33] correlation. For a fair comparison, the bubble size predicted from the Werther[30] correlation is used in their bubble rise velocity correlation. At this fixed height, the bubble rise velocity increases with increase in bed diameter, where the observed bubble rise velocity is in closest agreement with Hilligardt and Werther correlation for the 0.60 m diameter bed.

Figure 15b shows the bubble rise velocity as a function of height in the bottom section of a 1.0 m diameter bed. As expected, the bubble rise velocity increases because the bubbles grow with increasing height. The Hiligardt and Werther correlation show a closed match at heights of 0.09 and 0.14 m, but above this height the simulations predict a higher bubble rise velocity. This is due to the gulf stream phenomenon, dominating above this height. Furthermore, the collision characteristics of solids used here (LLDPE) lead to a higher gas holdup, resulting in higher bubble rise velocities at higher heights, as reported in our previous experimental and simulation study.[23] Matsen[5] argued that in a large bubbling FB, a gulf stream concentrates gas bubbles in the center of the bed and greatly affects their velocity. The bubble rise velocity and bed densities in such cases cannot be calculated directly from knowledge of the superficial gas velocity and bubble size. This is also remarkable from our simulation results for larger bed diameters. Overall, the analysis of bubble rise velocity for different bed diameters confirms that the bubbles rise much faster in the larger beds.

Solids circulation patterns

Solid particles are dragged up by the bubbles in their wakes and, by continuity, particles will move downwards in the regions with no or less bubbles. As a consequence, a predominantly downward flow of solids exists in regions of less activity of bubbles, most notably near the wall. As seen from the experimental comparison of solids circulation (Figure 3), the solids motion is upwards in the center and

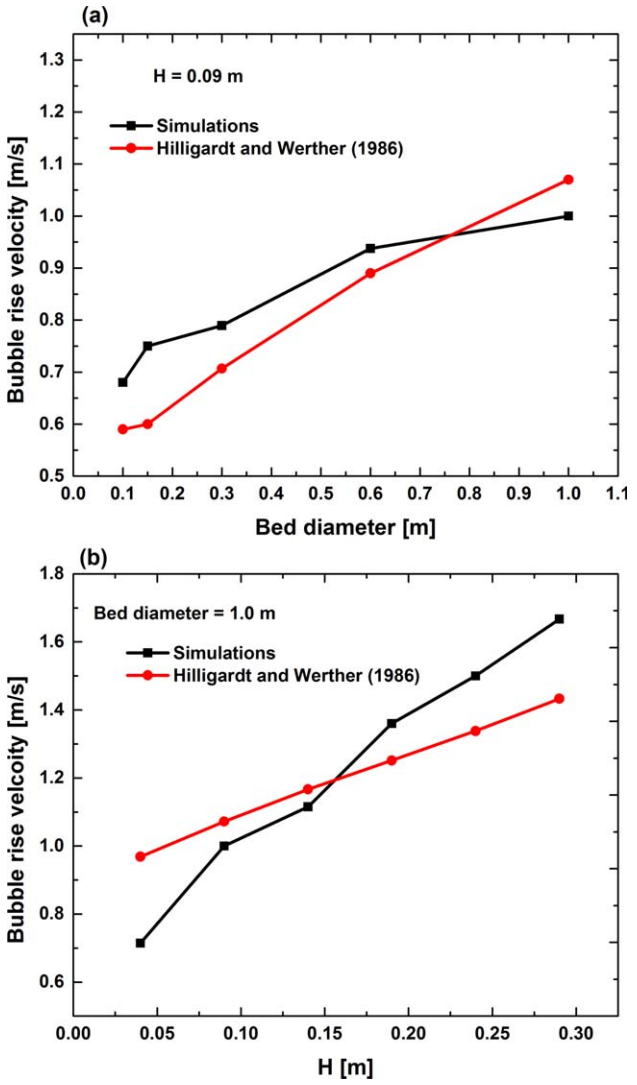

Figure 15. The bubble rise velocity for (a) different bed diameter at fixed height of 0.09 m from the bottom, and (b) bed diameter of 1.0 m at different axial position.

[Color figure can be viewed in the online issue, which is available at wileyonlinelibrary.com.]

downwards near the wall in the higher regions; the converse is true in the lower regions.

Figure 16 shows the azimuthally and time-averaged solids circulation patterns in FBs with diameters of 0.10, 0.15, 0.30, 0.60, and 1.0 m respectively. The simulations predict two different solids circulation vortices for all bed diameters, with differences in the vortex configurations. The center of the solids circulation vortex at the bottom lies near the wall. This shows that the initial bubble formation is occurring predominantly close to the wall, as already mentioned in our earlier explanation of the porosity plots. The increase in bed diameter eventually allows initial bubble formation even relatively closer to the wall. The upper solids circulation is elongated in smaller beds. The magnitude of solids velocity is much higher in smaller beds. This is attributed to slugging behavior in the top section of a smaller bed, as the bed height is sufficiently deep compared to the bed diameter. In the slugging region, the solids move with the roof top of the bubble approximately equal to the bubble rise velocity. However, in larger beds the solids are mostly carried through the wakes of the bubble. As the bed diameter is increased from 0.30 to 0.60 and to 1.0 m, the solids move with higher velocity due to the increase in bubble size and bubble rise velocity. The lower vortex of solids circulation gets enlarged and horizontally elongated as the bed size is increased, again caused by the larger bubble size in the larger bed. The upper vortex in the bed of 1.0 m is at a height comparable to the initial particle bed height, indicating gulf stream circulation as suggested by Merry and Davidson.[46] They suggest these gulf streams are introduced with an uneven distribution of gas. The bed of 1.0 m is tall enough to create compression of gas at the bottom, leading to an uneven gas distribution and these complicated toroidal gulf stream circulations of solids. Furthermore, the gulf stream circulations in the bed of 1.0 m is clearly reflected by the higher magnitude of solid

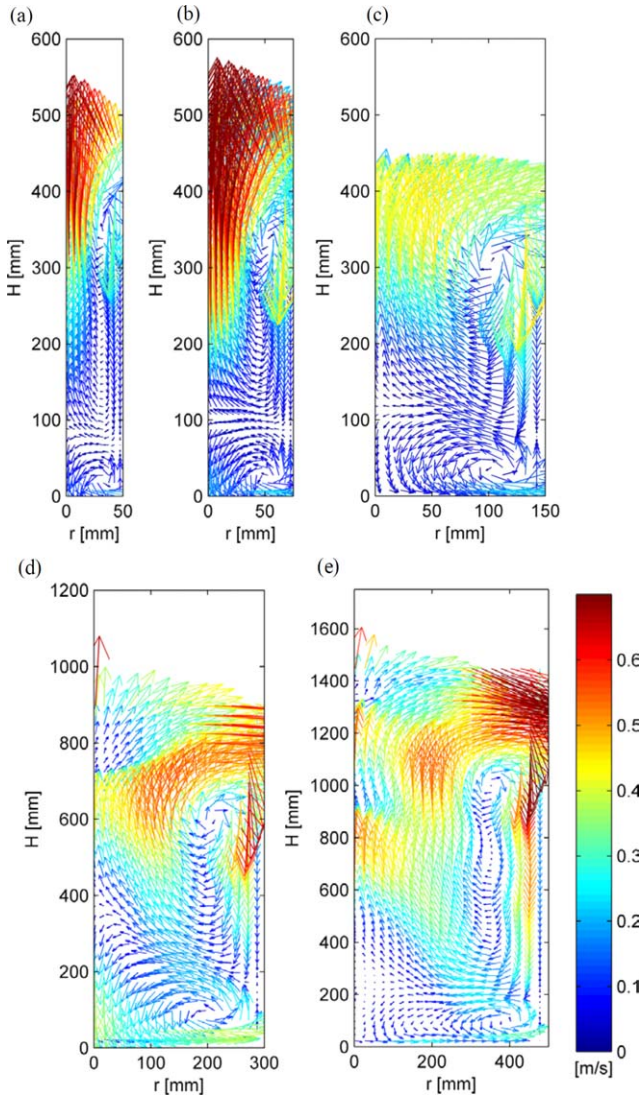

Figure 16. Azimuthally and time-averaged solids circulation patterns in (a) 0.10, (b) 0.15, (c) 0.30, (d) 0.60, and (e) 1.0 m diameter bed.

Initial particle bed height (h0) for (a–c) is 0.30 m, for (d) is 0.60 m, and for (e) 1.0 m. The color bar represent the magnitude of the solids velocity in m/s. For clarity only a reasonable number of vectors is shown. [Color figure can be viewed in the online issue, which is available at wileyonlinelibrary.com.]

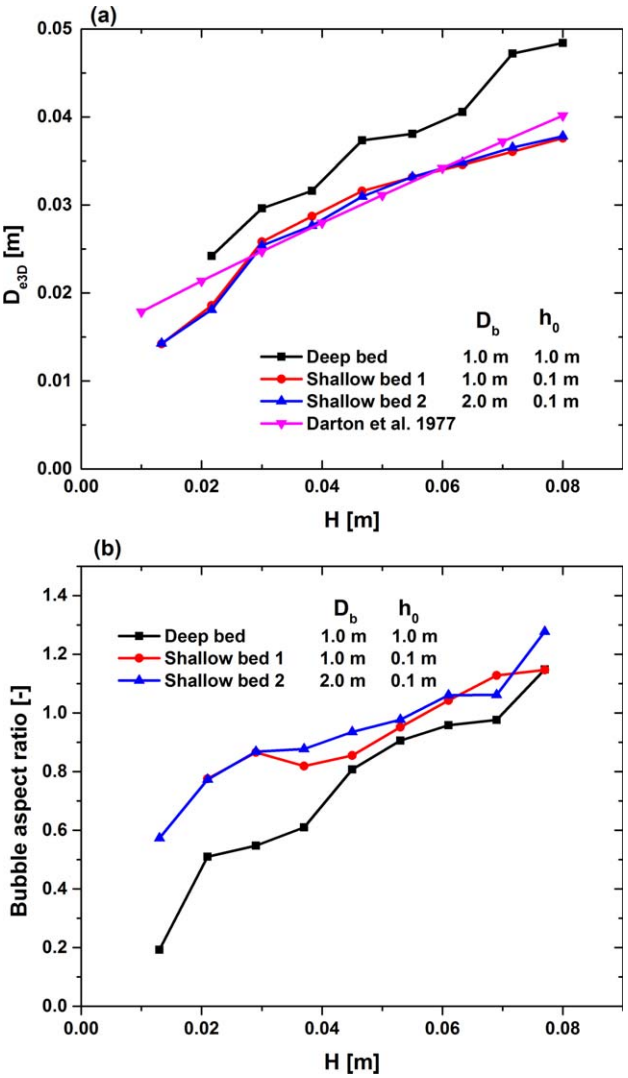

Figure 17. Comparison between shallow beds and a deep bed for (a) the equivalent bubble diameter and (b) the bubble aspect ratio, as a function of height from the bottom.

[Color figure can be viewed in the online issue, which is available at wileyonlinelibrary.com.]

velocity descending near the wall and ascending in the center. It should also be noted that in such deep beds the bubbles initiated from different directions have enough space and time for coalescence and breakup. This will create a more chaotic motion of the bubbles in the bed, resulting in the unique hydrodynamics when compared with small scale FBs. This type of gulf stream, as predicted in the bed of 1.0 m diameter, is preferred in industrial scale reactors to limit the self-segregation and promote mixing by carrying more solids to the top of the bed.[47] Unfortunately no experimental results concerning particle circulations in larger bubbling FBs are available.

Deep and shallow bed

Up to this point, we have focused on the influence of bed diameter in relatively deep beds, using an initial particle bed height of one or two bed diameters. Now we will investigate the hydrodynamics of FBs which in a sense are the opposite, namely very wide and shallow beds. From animations of

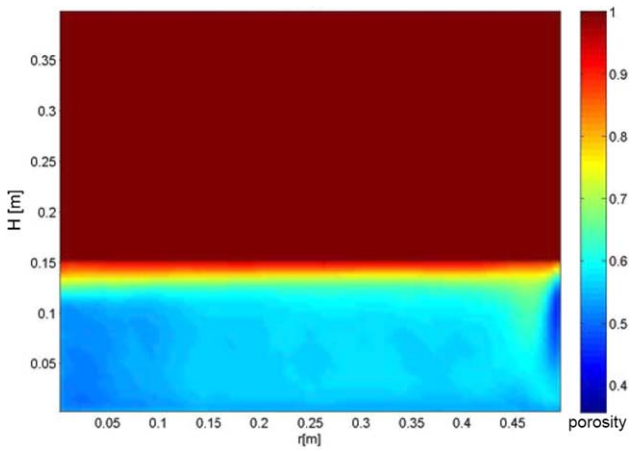

Figure 18. Azimuthally and time-averaged porosity plot in the shallow bed of diameter 1.0 m.

[Color figure can be viewed in the online issue, which is available at wileyonlinelibrary.com.]

such shallow beds, we observe a more intense gas bubbling in shallow beds, with a larger number of bubbles formed at the bottom. In shallow beds, the bubbles do not have sufficient room to fully develop on their way to the free surface. Let us now characterize the bubble development in the domain of interest, and compare it with a similar domain in a deep bed.

Figure 17a shows that bubble size predicted in a shallow bed is slightly lowered when compared with the bubble size in a deep bed with the same diameter. No significant difference in the bubble size is observed when the bed is even more shallow by increasing the diameter to 2.0 m. Proportionally, a decrease in bubble rise velocity is also predicted in a shallow bed (not shown). Furthermore, Figure 17b shows that bubbles have a flatter shape in the deep bed, which may be attributed to a higher pressure head due to the weight of the particle bed in the deeper bed. This can also explain the reason for the larger bubble size in a deep bed, as the bubble expands more in the lateral direction and has a better chance to coalesce with surrounding bubbles.

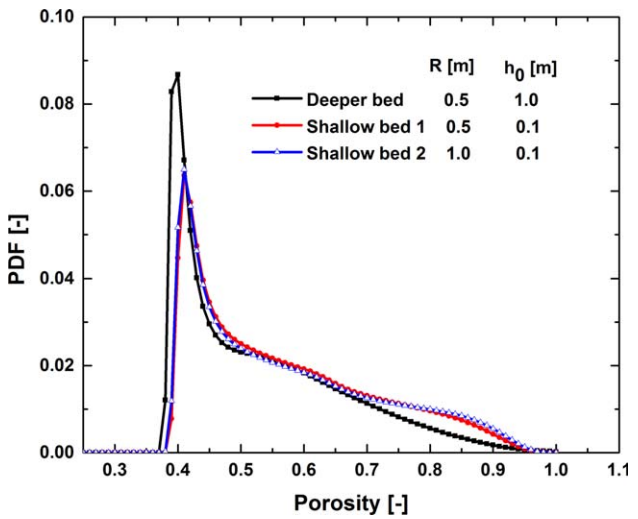

Figure 19. PDF comparison between shallow beds and a deep bed.

[Color figure can be viewed in the online issue, which is available at wileyonlinelibrary.com.]

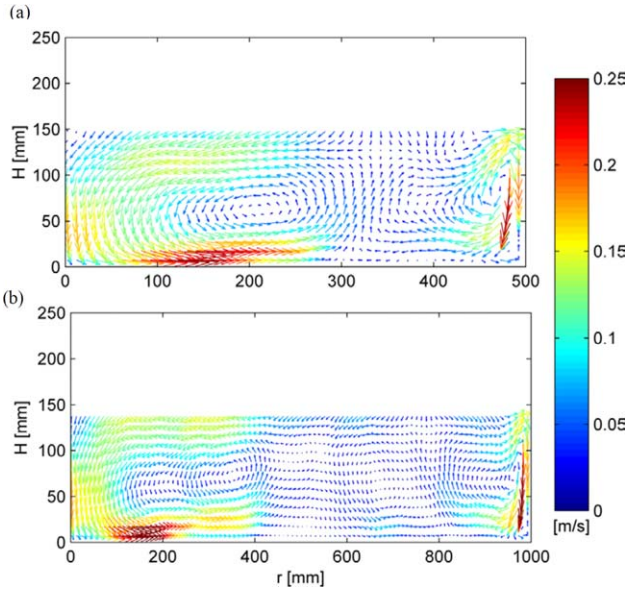

Figure 20. Azimuthally and time-averaged solids circulation in a shallow bed of diameter (a) 1.0 m and (b) 2.0 m.

The color bar represents the magnitude of the solids velocity in m/s. For clarity only a reasonable number of vectors is shown. [Color figure can be viewed in the online issue, which is available at wileyonlinelibrary.com.]

The time-averaged porosity in Figure 18 reveals that the porosity distribution is almost homogenous throughout in the shallow bed, except near the axis. Compared to a deep bed, dense particle zones are less evident, and spontaneous bubble formation is occurring all across the cross-section. This leads to a bubble rise predominantly in the vertical direction. This is also clear from the PDF plot in Figure 19 where a higher probability of dense emulsion phase is observed in the deep bed.

The solids circulation pattern in a shallow bed is very distinct from a deep bed. Figure 20 shows that an additional solids circulation vortex is formed near the wall in the 1.0 m diameter shallow bed. If the bed diameter is further increased to 2.0 m, the number of circulating zones increases correspondingly. The magnitude of the solids velocity is higher near the axis region for both shallow beds.

Conclusions

The effect of bed diameter on bubble and solids motion has been investigated using a TFM based on KTGF. The solids volume fraction near the wall is higher for a bed diameter of 1.0 m and gradually decreases in relatively smaller beds. In this work, we propose that the effective bubble diameter should be calculated taking into account the actual 3-D volume of the bubble. The bubble size predicted from bubble pierce length or from horizontal cross-sectional area of the bubble, is not accurate for bed diameters greater than 0.15 m. The bubble size generally increases with increasing bed diameter. A significant difference in the bubble size is predicted when increasing the bed diameter from 0.15 to 0.30 m. The bubble size in a bed of diameter 0.30–1.0 m does not show any significant difference. However, the bubbles rise much faster in the larger bed diameter. Most notably, the motion of bubbles in a 1.0 m diameter bed is much faster due to gulf stream circulations. Whether the bubbles reach the center of the bed depends on the bed height and diameter. The height of the initial solids bed should be at least equal to the diameter of the bed for the bubbles to reach the center. Slugging bubbles are predicted for a bed diameter of 0.10 m above a height of 0.20 m from the bottom. Very similar bubbles characteristics are predicted for bed diameters of 0.30, 0.60, and 1.0 m. This shows that a leveling off is predicted for a bed diameter laying between 0.30 and 0.60 m. Different particle circulation patterns are observed in different sized beds. To a certain extent similar particle circulation patterns are seen in beds of 0.30 and 0.60 m diameter. However, very distinct gulf stream circulation vortices equal to the bed height are predicted in the bed of diameter 1.0 m. This is further evidence that the hydrodynamics change between very small beds to intermediate beds, and further changes occurs between intermediate beds and very large beds.

In shallow beds, the porosity distribution is homogenous and relatively smaller bubbles arise compared to a much deeper bed. Increases in solids circulating zones are predicted if the bed is shallow.

A comparison with experimental results shows that our simulations show best agreement when using a very fine grid size. Nevertheless, this study provides a critical comparison for five different bed diameters. Further experimental work is highly recommended in this area. From this study, we can conclude that the TFM can be used to investigate gas–solids flow in a pilot plant scale FB. This will facilitate a rational scale-up to life-size FB reactors.

Acknowledgment

The authors would like to thank the European Research Council for its financial support, under its Advanced Investigator Grant scheme, contract number 247298 (MultiscaleFlows).

Notation

C = fluctuation particle velocity, m·s^{-1}
g = gravitational acceleration, m·s^{-2}
I = unit tensor,
p = pressure, Pa
q = kinetic fluctuation energy, kg·s^{-1}
u = velocity m·s^{-1}
t = time, s
e_n = coefficient of restitution,
U_{mf} = minimum fluidization velocity, m·s^{-1}
A = area of bubble, m^2
V = bubble volume, m^3
D = equivalent bubble diameter, m
H = height from the bottom/distributor, m
R = radius of the bed, m
r = radial position in the bed, m
Z = axial position of bubble, m
X = lateral position of bubble, m

Greek letters

β = interphase momentum transfer coefficient, kg·m^{-3}·s^{-1}
γ = dissipation due to inelastic particles collisions, kg·m^{-1}·s^{-3}
ε = volume fraction
ρ = density, kg·m^{-3}
Θ = pseudo particle temperature, m^2·s^{-2}
τ = stress tensor, Pa
μ = shear viscosity, kg·(m·s)$^{-1}$

Subscripts

s = solid phase
g = gas phase
p = particle
b = bubble

mf = minimum fluidization
e = equivalent
eH = equivalent from horizontal cross-sectional plane
eV = equivalent from central vertical plane
*e*3-D = equivalent from 3-D bubble volume
max = maximum
min = minimum

Literature Cited

1. Van Swaaij WPM. Chemical reactor. In: Davidson JF, Clift R, and Harrison D, editors. *Fluidization, 2nd ed.* London: Academic Press, 1985:595–629.
2. Squires AM. Contribution towards a history of fluidization. In: *Proceeding of the Joint Meeting of Chemical Engineering society of China and AIChE*, Beijing, China, Chemical Industry press, 1982: 322–353.
3. Fitzgerald T, Bushnell D, Crane S, Shieh, Y-C. Testing of cold scaled bed modeling for fluidized-bed combustors. *Powder Technol.* 1984;35:107–110.
4. Rudisuli M, Schildhauer TJ, Biollaz SMA, van Ommen RJ. Scale-up of bubbling fluidized bed reactor—a review. *Powder Technol.* 2012; 217:21–38.
5. Matsen, JM. Scale-up of fluidized bed processes: principle and practice. *Powder Technol.* 1996;88:237–244.
6. van Ommen RJ, Teuling M, Nijenhuis J, van Wachem BGM. Computational validation of the scaling rules for fluidized beds. *Powder Technol.* 2006;163:32–40.
7. Sierra C, Tadrist L, Occelli R. Local and global dynamics of shallow gas-fluidized beds. *Phys fluids* 2006;18:043303.
8. Krishna R, van Baten JM, Urseanu MI, Ellenberger J. Design and scale up of bubble column slurry reactor for Fischer-Tropsch synthesis. *Chem Eng Sci.* 2001;56:537–545.
9. Chen W, Hasegawa T, Tsutsumi A, Otawara K. Scale up effects on the time-averaged and dynamic behavior in bubble column reactors. *Chem Eng Sci.* 2001;56:21–22, 6149–6155.
10. Werther J. Influence of bed diameter on the hydrodynamics of gas fluidized beds. *AIChE Symp Ser.* 1974;70:53–62.
11. Glicksman LR, McAndrews G. The Effect of bed width on the hydrodynamics of large particle fluidized beds. *Powder Technol.* 1985;42:159–167.
12. Glicksman LR, Hyre M, Woloshun W. Simplified scaling relationships for fluidized beds. *Powder Technol.* 1993;77:177–199.
13. Glicksman LR. Scaling relationship for fluidized beds. *Chem Eng Sci.* 1984;39:1373–1379.
14. Knowlton TM, Karri SBR, Issangya A. Scale-up of fluidized-bed hydrodynamics. *Powder Technol.* 2005;150:72–77.
15. Rüdisülia M, Schildhauer TJ, Biollaz SMA, van Ommen RJ. Scale-up of bubbling fluidized bed reactors—a review. *Powder Technol.* 2012;217:21–38.
16. Werther J. Scale-up modeling for fluidized bed reactors. *Chem Eng Sci.* 1992;47:9–11, 2457–2462.
17. Laverman JA, Fan X, Ingram A, van Sint Annaland, M, Parker DJ, Seville JPK, Kuipers JAM. Experimental study on the influence of bed material on the scaling of solids circulation patterns in 3D bubbling gas-solid fluidized beds of glass and polyethylene using positron emission particle tracking. *Powder Technol.* 2012;224:297–305.
18. Ding J, Gidaspow D. A bubbling fluidization model using kinetic theory of granular flow. *AIChE J.* 1990;36:523–538.
19. Kuipers JAM, van Duin KJ, van Beckum FPH, van Swaaij WPM. A numerical model of gas-fluidized beds. *Chem Eng Sci.* 1992;47: 1913–1924.
20. Gidaspow D. *Multiphase Flow and Fluidization: Continuum and Kinetic Theory Descriptions.* Boston: Academic Press, 1994.
21. Nieuwland JJ. *Hydrodynamic Modelling of Gas-Solid Two-Phase Flows.* Ph.D. Thesis, Enschede, The Netherlands: Twente University, 1995.
22. Verma V, Deen NG, Padding JT, Kuipers JAM. Two-fluid modeling of three-dimensional cylindrical gas–solid fluidized beds using the kinetic theory of granular flow. *Chem Eng Sci.* 2013;102:227–245.
23. Verma V, Padding JT, Deen NG, Kuipers JAM, Bieberle M, Barthel F, Wagner M, Hampel U. Bubble dynamics in a 3-D gas–solid fluidized bed using ultrafast electron beam X-ray tomography and two-fluid model. *AIChE J.* 2014;60:1632–1644.
24. Levenspiel O. Difficulties in trying to model and scale-up the bubbling fluidized bed (BFB) reactor. *Ind Eng Chem Res.* 2008;47;272–277.
25. Brouwer GC, Wagner EC, van Ommen JR, Mudde RF. Effects of pressure and fines content on bubble diameter in a fluidized bed studied using fast x-ray tomography. *Chem Eng J.* 2012;207–208: 711–717.
26. Mudde RF. Time-resolved x-ray tomography of a fluidized bed. *Powder Technol.* 2010;199:55–59.
27. Hulme I, Kantzas A. Determination of bubble diameter and axial velocity for a polyethylene fluidized bed using X-ray fluoroscopy. *Powder Technol.* 2004;147:20–33.
28. Saayman J, Nicol W, van Ommen RJ, Mudde RF. Fast X-ray tomography for the quantification of the bubbling-, turbulent- and fast fluidization-flow regimes and void structures. *Chem Eng J.* 2013; 234:437–447.
29. Darton RC, La Naueza RD, Davidson JF, Harrison D. Bubble growth due to coalescence in fluidized beds, *Trans Inst Chem Eng.* 1977;55:274–280.
30. Werther J, Bubble growth in large diameter fluidized beds. International Fluidization conference, Pacific Grove, USA, 1975, In: Keairns DL, editor, Fluidization Technology, Hemisphere Publ. Co., Washington DC, 1976:215–235.
31. Godlieb W, Gorter S, Deen NG, Kuipers JAM. Experimental study of large scale fluidized beds at elevated pressure. *Ind Eng Chem Res.* 2012;51:1962–1969.
32. Werther J, Molerus O. The local structure of gas fluidized beds-I. *A statistically based measuring system. Int J Multiphase flow.* 1973;1: 103–122.
33. Hilligardt K, Werther J. Local bubble gas hold-up and expansion of gas/solid fluidized beds. *Ger Chem Eng.* 1986;9:215–221.
34. van der Hoef MA, Beetstra R, Kuipers JAM. Lattice-Boltzmann simulations of low-Reynolds number flow past mono- and bidisperse arrays of spheres: results for the permeability and drag force. *J Fluid Mech.* 2005;528:233–254.
35. Srivastava A, Sundaresan S. Analysis of a frictional-kinetic model for gas-particle flow. *Powder Technol.* 2003;129:72–85.
36. Wen CY, Yu YH. Mechanics of fluidization. *AIChE. Series* 1966;62, 100–111.
37. Ergun S. Fluid flow through packed columns. *Chem Eng Proc* 1952; 48:89.
38. Bokkers GA. *Multi-Level Modelling of the Hydrodynamics in Gas Phase Polymerization Reactors.* Ph.D. Thesis, The Netherlands: Twente University, Enschede, 2005.
39. Andrews IV AT, Loezos PN, Sundaresan S. Coarse-grid simulation of gas-particle flows in vertical risers. *Ind Eng Chem Res.* 2005;44: 6022–6037.
40. Igci Y, Pannala S, Benyahia S, Sundaresan S. Validation studies on filtered model equations for gas-particl flows in risers. *Ind Eng Chem Res.* 2012;51:2094–2103.
41. Cranfield RR, Geldart D. Large particle fluidization. *Chem Eng Sci.* 1974;29:935–947.
42. Kunii D, Levenspiel O. Fluidization Engineering, 2nd ed. Butterworth-Heinemann, Inc, Boston, 1991.
43. Stefanova A, Bi HT, Lim JC, Grace JR. Local hydrodynamics and heat transfer in fluidized beds of different diameter. *Powder Technol.* 2011;212:57–63.
44. Volk W, Johnson CA, Stotler HH. Effect of reactor internals on quality fluidization. *Chem Eng Prog.* 1962;58(2):44–47.
45. Karimipour S, Pugsley T. A critical evaluation of literature correlations for predicting bubble size and velocity in gas–solid fluidized beds. *Powder Technol.* 2011;205:1–14.
46. Merry JMD, Davidson JF. Gulf-stream circulation in shallow fluidized-beds. *Trans. Instn. Chem Eng.* 1973;81:361–368.
47. Solimene R, Aprea G, Chirone R, Marzocchella A, Salatino P. Hydrodynamic characterization of "GULF STREAM" circulation in a pilot scale fluidized bed combustor. In: The 14th International Conference on Fluidization – From Fundamentals to Products, Kuipers JAM, Mudde RF, van Ommen JR, Deen NG, Eds, ECI Symposium Series, Volume (2013). Available at: http://dc.engconfintl.org/fluidization_xiv/112.

Manuscript received Apr. 3, 2014, and revision received Nov. 24, 2014.